IEEE Photonics Journal
An IEEE Photonics Society Publication

Open Access

3D Simple Monte Carlo Statistical Model for GaAs Nanowire Single Photon Avalanche Diode

Volume 12, Number 4, August 2020

Shiyu Xie
Haochen Li
Jamal Ahmed
Diana L. Huffaker

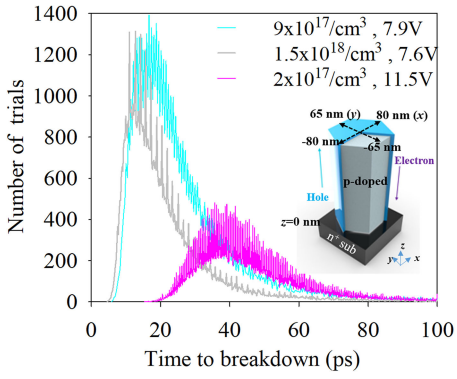

DOI: 10.1109/JPHOT.2020.3006957

3D Simple Monte Carlo Statistical Model for GaAs Nanowire Single Photon Avalanche Diode

Shiyu Xie, Haochen Li, Jamal Ahmed, and Diana L. Huffaker

School of Physics and Astronomy, Cardiff University, Cardiff, CF24 3AA, UK

DOI:10.1109/JPHOT.2020.3006957

Manuscript received May 21, 2020; revised June 24, 2020; accepted June 29, 2020. Date of publication July 3, 2020; date of current version July 14, 2020. This work was supported by European Regional Development Fund (ERDF 80762-CU-039). Corresponding author: Shiyu Xie (email: xies1@cardiff.ac.uk).

Abstract: GaAs based nanowire single photon avalanche diode (SPAD) has been demonstrated with extremely small afterpulsing probability and low dark count rate, and hence it has attracted wide attention for the near infrared applications. However, there is a lack of model to accurately evaluate the avalanche breakdown performance in nanowire SPAD with a spatially non-uniform electric field. In this work, we have developed a three-dimensional (3D) Simple Monte Carlo statistical model for GaAs nanowire SPADs. Model validation includes ionisation coefficients of GaAs and avalanche gain in GaAs nanowire avalanche photodiode. We also apply our model to predict the device performances of breakdown probability, mean time to breakdown and timing jitter, which are essential parameters for SPAD design. Simulating a PN junction GaAs nanowire SPAD design using our model, we found that device performances have little dependence on the primary carrier injection type, but the nanowire doping concentration requires optimization for high performance SPAD design and operation.

Index Terms: GaAs, Monte Carlo, Nanowire, Single Photon Avalanche Diode.

1. Introduction

Single photon avalanche diodes (SPADs), also known as Geiger-mode avalanche photodiodes (APDs), operating at near infrared wavelength are vital optical components used for various applications, such as time-resolved photon counting [1], light detection and ranging (LIDAR) [2], and quantum key distribution [3]. Today's near-infrared SPADs rely on InGaAs/InP separate absorption-multiplication (SAM) structures, but their high dark count rate and afterpulsing probability limit their commercial applications [4], [5]. Planar Ge-on-Si SPAD has been reported to have a considerably reduced afterpulsing effects, but the Ge/Si lattice mismatch makes the layer growth much more difficult than typical InGaAs-InP SPADs [6], [7].

Recently GaAs-based nanowire APDs and SPADs have been demonstrated experimentally with impressive properties including large lattice mismatch accommodation, low dark current and high avalanche gain in the near infrared regime [8], [9] due to its very small active volume compared to its planar counterpart. For instance, Senanayake et al. reported a GaAs nanowire APD [8] with high avalanche gain above 100. Farrell et al. demonstrated an InGaAs/GaAs nanowire SPAD [9] utilizing GaAs as avalanche gain material which exhibits an extremely small afterpulsing probability and low dark count rate. Hence, the development of a model that is capable of interpreting the avalanche

breakdown performance for GaAs based nanowire APD/SPAD will be useful for high performance device design and optimization.

Due to the spatially non-uniform electric field intensity across and along nanowire APD/SPADs, it requires an accurate description on the carrier impact ionization process [10]. However, the conventional local ionization model [11] is unable to deal with rapidly changing electric field and does not take into account the history of the carriers. Random Path Length model [12] is more accurate than the conventional local model in a statistical way, but it relies critically on accurate descriptions of the ionization path length probability density functions (PDFs) as input parameters. These PDFs are difficult to parameterize when the electric field is rapidly changing, making it useful only in devices with near constant electric fields. Recently, a three-dimensional (3D) dead space multiplication theory model has been developed [13] to analyse the avalanche gain and excess noise result in nanowire APD. However, to our knowledge the authors have not used it for the simulation of nanowire SPADs yet.

Simple Monte Carlo (SMC) statistical model has been benchmarked extensively with experimental data on impact ionization for Si bulk APD [14] and SAPD [15] on one-dimensional (1D) simulation. It contains far less band structure details compared to full band Monte Carlo model, and includes carrier scattering mechanism (including impact ionization) updated on a femtosecond timescale, so that it can handle highly non-uniform electric field [15] with shorter simulation time. In this work, we built up a 3D SMC statistical model for GaAs nanowire SPAD. Our model is capable of predicting the avalanche multiplication process, breakdown probability, mean time to breakdown and timing jitter. Device structure with PN junction is evaluated with our model Both effects of varying the nanowire doping concentration and the primary carrier injection type are investigated.

2. Model Description and Validation

The SMC statistical model contains three scattering mechanisms: phonon absorption, phonon emission, and impact ionization [16]. A charge carrier drifts in the electric field so that it will gain energy during the free flight, and then the flight will end with either a scattering or an impact ionization event. The probability to choose one of these options depends on normalized scattering rates. To determine the carrier scattering options, a random number between 0 and 1 is generated that selects the scattering mechanism based on its corresponding probability of occurrence. This process is repeated at each scattering event and carrier energy and momentum are updated based on the selected scattering mechanism. Here the complicated band structure is simplified to a parabolic band and the standard rate equations are employed to obtain these three scattering rates [17]. The first two scattering rates, phonon absorption and phonon emission, can be characterized by a phonon mean free path λ, a phonon energy $\hbar\omega$ and an effective mass m^*, the phonon scattering rate is given by following equations:

$$R_{ph} = C_{ph}\,(2N+1)\,\varepsilon_f^{1/2}$$

Where $C_{ph} = (\frac{2}{m^*})^{\frac{1}{2}}/(\lambda(2N+1))$, $N = (\exp(\frac{\hbar\omega}{kT}) - 1)^{-1}$ is the phonon occupation number, k is the Boltzmann's constant, T is the absolute temperature and $\varepsilon_f = \varepsilon + \hbar\omega$ for absorption or $\varepsilon_f = \varepsilon - \hbar\omega$ for emission is the final energy of the carrier with the initial energy ε. The single phonon energy $\hbar\omega$ based on Ridley's common phonon model is used to quantitatively describe collisions between charge carriers and lattices, which is also the energy exchange between carriers and lattices. The impact ionization rate is introduced as an additional scattering mechanism. If it occurs, one single charge carrier will transforms into three carriers, the initial carrier and a new-produced electron-hole pair, the final energy of these three carriers is $\varepsilon_f = \frac{\varepsilon - E_{th}}{3}$. The impact ionization rate, R_{ii} was described by conventional Keldysh rate [18] formula as

$$R_{ii} = C_{ii} \times \left(\frac{\varepsilon - E_{th}}{E_{th}}\right)^{\gamma}$$

where C_{ii} is a coefficient for impact rate, γ is the ionization rate softness factor and E_{th} is the impact ionization threshold energy.

TABLE 1
Parameters Used in the Model [17]

Parameters (unit)	Electron	Holes
Phonon energy $\hbar\omega$ (meV)	29	29
Threshold energy E_{th} (eV)	1.75	1.75
Maximum Energy$E_{th,max}$ (eV)	5.25	5.25
Free path length λ (Å)	50.4	47.6
Impact ionization rate coefficient C_{ii} (s^{-1})	4×10^{13}	3×10^{13}
Softness factor γ	4	4
Effective mass m^* (kg)	$0.5m_o$	$0.5m_o$

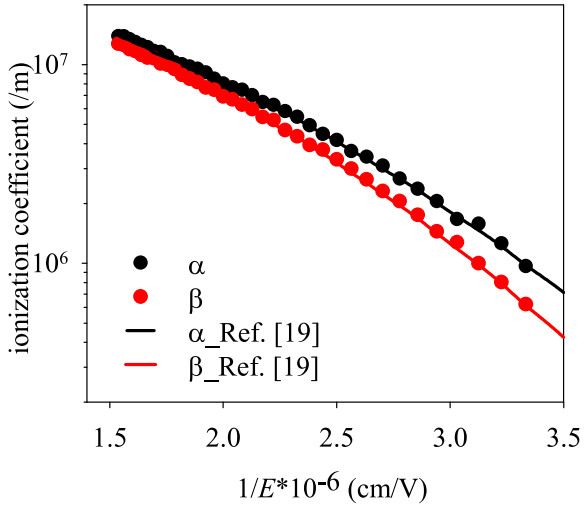

Fig. 1. Our modelled (symbols) and experimental data from Ref. [19] (solid lines) of electron (α) and hole (β) ionisation coefficients for GaAs at 300 K.

We firstly built up a SMC model with constant electric fields utilizing the parameters of GaAs in Table 1 [17]. The calculated electron and hole ionization rates of GaAs from our model fit the experimental data [19] very well at 300K, as shown in Fig. 1. Then, we further develop a 3D statistical model to simulate the avalanche gain in ideal GaAs nanowire APDs. Hexagonal-shaped GaAs nanowire (160 nm (x) x 130 nm (y) in width, 1000 nm (z) in height) with p type background doping on n+ GaAs substrate was considered, as shown in Fig. 2(a). A commercial software, Lumerical Device [20], was used to calculate 3D discretization mesh of 10 nm (x) $\times$ 10 nm (y) $\times$ 1 nm (z) and output is generated as the 3D non-uniform electric field profile in GaAs nanowire APD/SPAD. This 3D electric field data was used as input parameter into our model and a primary carrier is then randomly injected onto the top surface of the nanowire (or the bottom of the substrate) with 17 (x) x 14 (y) paths calculated along z axis. The carrier will subsequently diffuse into the depletion region to undergo the phonon scattering or impact ionization process. Due to the highly non-uniform 3D electric field profile, the carriers at different possible paths will experience distinct impact ionization process. Using a large number of simulations with 100,000

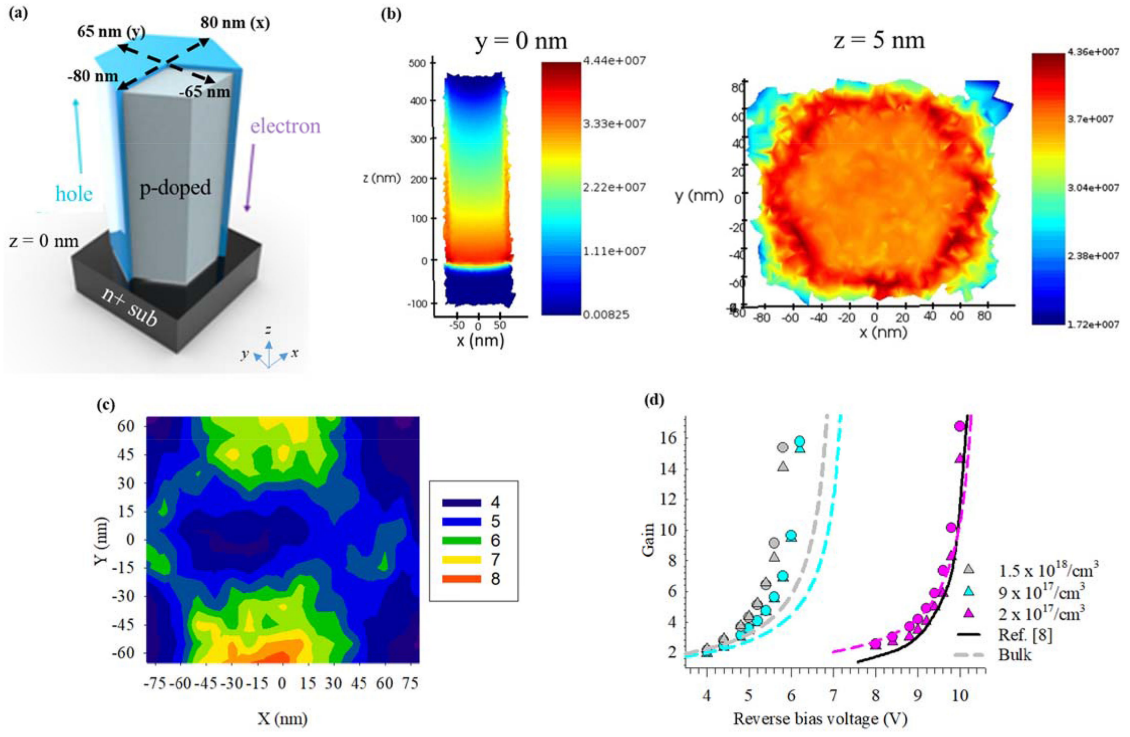

Fig. 2. (a) Schematic of GaAs nanowire APD/SPAD structure and (b) an example of the output x-z electric field profile (left) and x-y electric field (V/m) profile at z = 5 nm (right) for GaAs nanowire APD generated from Lumerical device simulation software using doping concentration of $2 \times 10^{17}/\text{cm}^3$ and reverse bias voltage of 9 V; (c) the corresponding x-y contour map of the gain distribution under electron injection; (d) modelled overall mean gain for GaAs nanowire APD versus reverse bias voltage with different nanowire doping and primary carrier injection type. Three p-doping concentration of $2 \times 10^{17}/\text{cm}^3$ (color: pink), $9 \times 10^{17}/\text{cm}^3$ (color: cyan) and $1.5 \times 10^{18}/\text{cm}^3$ (color: grey) with both electron (symbol: circle) and hole injection (symbol: triangle) were calculated. Experimental data (solid line) from Ref. [8] is also included for comparison. Modelling of $<M_h>$ in bulk structures with only z-axis non-uniform electric field by solving 1D Poisson equation is also included (dashed lines).

trials with random injection on the x-y grid at each voltage bias, the mean number of electrons or holes collected at the end of the multiplication process is different in each multiplication trajectory of the path simulated. Fig. 2(b) show an example of the output x-z electric field profile at y = 0 and x-y electric field profile at z = 5 nm from Lumerical Device for GaAs nanowire APD with nanowire doping concentration of $2 \times 10^{17}/\text{cm}^3$ and at reverse bias of 9 V. The corresponding x-y contour map of the gain distribution (mean number of carriers collected) over all possible routes with electron primary carrier injection is calculated from our model and the result is shown in Fig. 2(c). The x-y gain distribution is also hexagonal-shaped and identical to our nanowire dimensions. There is a clear edge effect leading to higher gain values compared to that of the center area due to the non-uniform electric field at the edge of the active area. By averaging this x-y contour map of gain distribution result, the overall mean gain, $<M_h>$ (or $<M_e>$), can be computed.

Fig. 2(d) shows our calculated voltage dependence of overall mean gain for GaAs nanowire APD with different nanowire doping and different primary carrier injection type. Three p-doping concentrations of $2 \times 10^{17}/\text{cm}^3$, $9 \times 10^{17}/\text{cm}^3$ and $1.5 \times 10^{18}/\text{cm}^3$ in nanowire are employed for both primary hole (from bottom of the substrate) and electron (from top surface of the nanowire) injection. Relatively high nanowire doping concentration was used in the model as high surface state density in nanowires leads to a high background doping [21]. Our calculated $<M_h>$ for nanowire doping concentration of $2 \times 10^{17}/\text{cm}^3$ shows good agreement with the experimental data

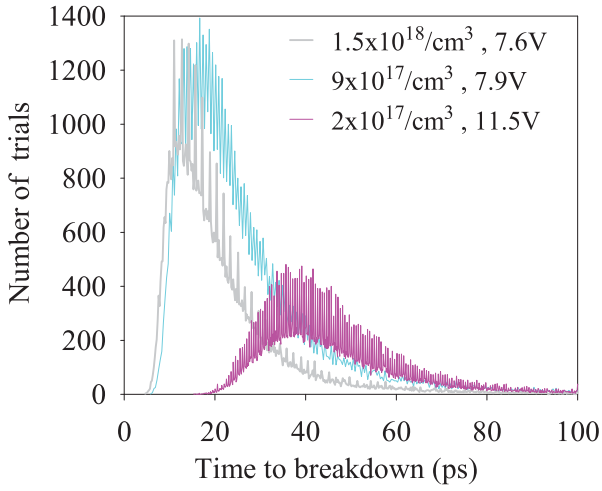

Fig. 3. An example of the distribution of the time to breakdown for GaAs nanowire SPAD with different p type doping concentration.

from Ref. [8] which has similar nanowire doping concentration. The agreement suggests our 3D SMC statistical model has ability to accurately simulate the avalanche gain in nanowire APDs. We noticed that the calculated $<M_e>$ is slightly higher than $<M_h>$ at nanowire doping concentration of $2 \times 10^{17}/\text{cm}^3$, but $<M_e>$ and $<M_h>$ shows more similar values at higher nanowire doping concentration. This is possibly due to the increase in operating field with the nanowire doping concentration, so that the electron and hole ionization rates approach more similar values at high fields, as shown in Fig. 1. We also simulated $<M_h>$ assuming that it is a bulk structure with only z-axis non-uniform electric field by solving 1D Poisson equation. However, this calculated $<M_h>$ at the doping concentration of $2 \times 10^{17}/\text{cm}^3$ cannot fit the experimental data well [8], and the result is also shown in Fig. 2(d), which suggests the necessity of our model to account for the 3D non-uniform electric field profile in nanowire structures. It is also clear to see that the nanowire device with 3D non-uniform electric field profile has a lower operating voltage compared to that in bulk device, when at the doping concentration of $9 \times 10^{17}/\text{cm}^3$ and $1.5 \times 10^{18}/\text{cm}^3$.

3. Results and Discussion

We further explore our model to investigate GaAs nanowire SPAD with a similar geometry and structure as shown in Fig. 2(a). The above mentioned three p-type nanowire doping concentrations were evaluated for both primary electron and hole injection. A detection threshold current is set to be $I_{th} = 5 \times 10^{-4}$ A with 100,000 simulation trials. The instantaneous avalanche currents contributed by each of the carriers can be computed using Ramo's theorem, $I = qV_s/w$ where q is the charge of an electron, V_s is a constant high field saturated drift velocity for both electrons and holes with the values of 6.2×10^4 and 6×10^4 m/s, respectively [22], [23], and w is the total depletion width.

Breakdown probability, P_b, which is strongly correlated with detection efficiency, was calculated as the ratio of the number of trials triggering breakdown to the number of total trials. The mean time required for the avalanche current to reach I_{th} is also calculated as the mean time to breakdown, t_b, and the timing jitter $\sigma = \sqrt{\sum (t - t_b)^2/n}$ was taken as the standard deviation of the mean time to breakdown. Here we neglect the carrier diffusion time to the depletion region. This is characteristic of avalanche breakdown timing performance which is important in SPADs, for instance small σ are desirable in time-correlated photon counting applications and the current high-timing-resolution of free-space SPADs is $\sigma \sim 35$ ps [25]. Fig. 3 shows an example of our

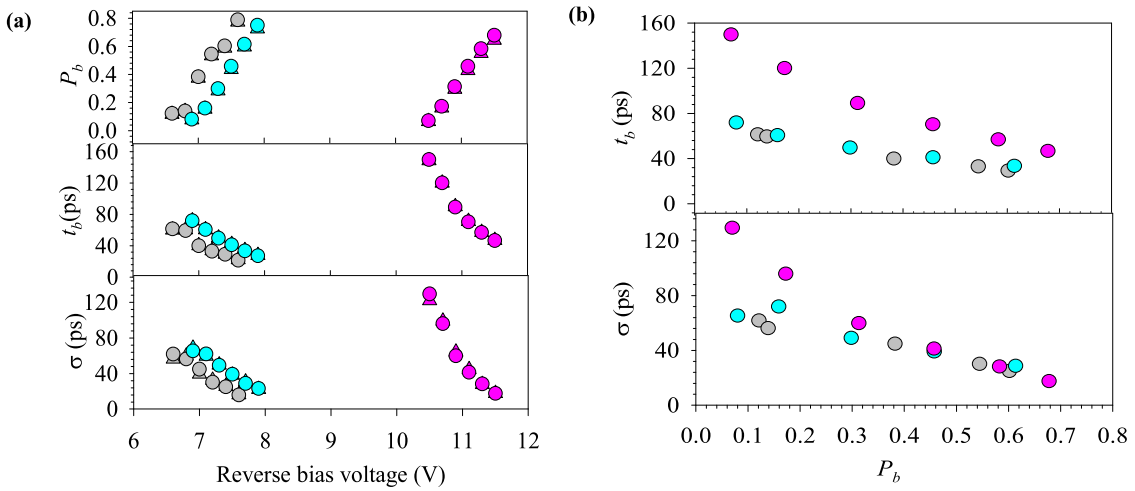

Fig. 4. Modelled (a) P_b (V), $t_b(V)$ and $\sigma(V)$ and (b) $t_b(P_b)$ and (b) $\sigma(P_b)$ for GaAs nanowire SPADs with p-doping concentration of $2 \times 10^{17}/\text{cm}^3$ (color: pink), $9\times10^{17}/\text{cm}^3$ (color: cyan) and $1.5 \times 10^{18}/\text{cm}^3$ (color: grey) and with both electron (symbol: circle) and hole injection (symbol: triangle) respectively.

calculated distribution of the time to breakdown for the nanowire p type doping concentration of $2 \times 10^{17}/\text{cm}^3$, $9 \times 10^{17}/\text{cm}^3$,$1.5 \times 10^{18}/\text{cm}^3$ and at the reverse bias of 11.5 V, 7.9 V and 7.6 V, respectively. The calculated total number of trials to reach breakdown are 78834, 74979 and 67789, and therefore the corresponding P_b are approximately 0.788, 0.75 and 0.678, respectively. The calculated t_b are 31.6 ps, 20.4 ps, 17 ps, and σ are19 ps, 20.6 ps, 14.6 ps, respectively. The average simulation time is $\sim$20 hours at each voltage point using our in-house computer server (equipped with Intel x64 based processor and 32 GB RAM).

Fig. 4(a) shows the calculated P_b (V), $t_b(V)$ and $\sigma(V)$ respectively. The breakdown voltage, V_{br}, is defined as the voltage when $P_b = 0.01$. The calculated V_{br} is 10.2, 6.7 and 6 V at the nanowire doping concentration of $2 \times 10^{17}/\text{cm}^3$, $9 \times 10^{17}/\text{cm}^3$, $1.5 \times 10^{18}/\text{cm}^3$ corresponding to the device peak electric field of 707 kV/cm, 985 kV/cm and 1.07 MV/cm respectively. The V_{br} reduces with peak electric field and this lower operating voltage is due to the higher ionization coefficient rates at higher fields [26]. It is worth noting that high peak fields corresponding to $1.5 \times 10^{19}/\text{cm}^3$ and $9 \times 10^{17}/\text{cm}^3$ doping levels will generate band to band tunneling current densities [27] of 0.436 A/m^2 and 0.0515 A/m^2 respectively in GaAs based devices. This will lead to significant calculated tunneling current of 137 pA and 16 pA and the resultant dark count rates are 850 MHz and 100 MHz respectively in bulk SPAD devices with typical diameter of 20 μm (assuming all the dark carriers originating from tunneling current result in dark counts). However, due to small volume of nanowire devices, tunneling current is significantly reduced (6.37 fA and 0.75 fA respectively) leading to a smaller dark count rate of 40 KHz and 4.7 KHz. For the devices with $2 \times 10^{17}/\text{cm}^3$ doping level, the calculated tunneling current is so small that the corresponding to dark count rate is only a few Hz. This result is similar to our measured InGaAs/GaAs nanowire SPAD with dark count rate $<$10 Hz [9], suggesting the validation of our model for nanowire SPADs.

At $V > V_{br}$, P_b increases with V approaching a limit close to unity, while t_b and σ reduces with V for avalanche process speeding up [14] and less variation in avalanche breakdown timing statistics. It is clear to see that the operating voltage of the devices are all below 12 V, which can be used for low voltage operation. The calculated P_b, t_b and σ have little dependence on the primary carrier injection type for the three nanowire doping concentrations under consideration. This is different from the above avalanche gain result for GaAs nanowire APD with nanowire doping concentration of $2 \times 10^{17}/\text{cm}^3$ as shown in Fig. 2(d). It can be understood that SPAD operating above V_{br} has higher operating field and hence it has more similar ionization rates than that in APD. The little dependence on primary carrier injection suggests that we can design a plasmonic antenna

structure on top of the nanowire, which will be useful to increase absorption [28] in the small nanowire volume and offer tunable absorption [29] across the absorption spectrum by varying the array geometrical parameters. Utilising nanowire-plasmonic structure will be beneficial for high detection efficiency and multispectral application. For clarity, hereafter we only show results for electron injection.

As Tan *et al.* claimed that it is more appropriate to compare the timing statistics at fixed values of P_b rather than voltages [30], we compare the calculated $t_b(P_b)$ and $\sigma(P_b)$ as shown in Fig. 4(b). Both t_b and σ decreases with P_b. For a fixed P_b, t_b reduces when the nanowire doping increases from $2 \times 10^{17}/\text{cm}^3$ to $9 \times 10^{17}/\text{cm}^3$ which might be due to the higher value of ionisation coefficients at higher naonowire doping. At $P_b < 0.4$, σ shows the same trend as t_b. But at higher P_b values, σ is less dependent on the nanowire doping concentration. The SMC statistical model provides realistic description of carrier transport using single effectively parabolic valleys and accurately incorporates carriers' deadspace effect [15], [16] which may lead to similar jitter values at larger P_b. At $P_b > 0.5$, σ is less than 35 ps on all three counts, which can meet the requirement for time-resolution of free space SPADs. With even higher P_b, σ with less than 20 ps is comparable to that in superconducting nanowire single photon detectors (SNSPD) [31], while SNSPD is well known for excellent timing resolution but requiring intensive cooling with operating temperatures of a few Kelvin.

From our simulation results, increasing the nanowire doping concentration (and in turn, the electric field and reducing the depletion width) has the benefits of yielding a higher P_b, lower t_b and σ with a lower operating voltage. However this improvement become less significant as the nanowire doping concentration is higher than $9 \times 10^{17}/\text{cm}^3$, while Zener breakdown becomes dominant at very high electric fields and thus impede the performance of SPAD [32].

4. Conclusion

In conclusion, we have developed a 3D SMC statistical model for GaAs nanowire SPAD. Model validation includes ionisation coefficients of GaAs and avalanche gain in GaAs nanowire APD. The simulated device structure is a PN diode. Device performances by varying nanowire doping level and primary carrier injection type have been investigated. Nanowire-plasmonic structure is proposed for GaAs nanowire SPAD for its little dependence on primary carrier injection at nanowire doping ranging from $2 \times 10^{17}/\text{cm}^3$ to $1.5 \times 10^{18}/\text{cm}^3$. Through optimisation of nanowire doping concentration, devices with high breakdown probability, low timing jitter and a low operating voltage could be achieved simulatenously. Our model can also be introduced into other 3D device geometries, doping profile and temperatures, which are critical for high performance device design and operation.

Disclosures

The authors declare no conflicts of interest.

References

[1] A. Spinelli, L. M. Davis, and H. Dautet, "Actively quenched single-photon avalanche diode for high repetition rate time-gated photon counting," *Rev. Sci. Instrum.*, vol. 67, no. 1, pp. 55–61, 1996.
[2] P. Gatt, S. Johnson, and T. Nichols, "Geiger-mode avalanche photodiode ladar receiver performance characteristics and detection statistics," *Appl. Opt.*, vol. 48, no. 17, pp. 3261–3276, 2009.
[3] D. Stucki, G. Ribordy, A. Stefanov, H. Zbinden, and J. G. Rarity, "Photon counting for quantum key distribution with Peltier cooled InGaAs/InP APDs," *J. Mod. Opt.*, vol. 48, no. 1, pp. 1967–1981, 2001.
[4] G. Ribordy, N. Gisin, O. Guinnard, D. Stuck, M. Wegmuller, and H. Zbinden, "Photon counting at telecom wavelengths with commercial InGaAs/InP avalanche photodiodes: Current performance," *J. Mod. Opt.*, vol. 51, no. 9–10, pp. 1381–1398, 2004.
[5] P. A. Hiskett *et al.*, "Performance and design of InGaAs/InP photodiodes for single-photon counting at 1.55 μm," *Appl. Opt.*, vol. 39, no. 36, pp. 6818–6829, 2000.
[6] P. Vines *et al.*, "High performance planar germanium-on-silicon single-photon avalanche diode detectors," *Nature Commun.*, vol. 10, no. 1, pp. 1–9, 2019.

[7] R. E. Warburton *et al.*, "Ge-on-Si single photon avalanche diode detectors: Design, modelling, fabrication and characterization at wavelength 1310 and 1550 nm," *IEEE Trans. Electron. Devices*, vol. 60, no. 11, pp. 3807–3813, Nov. 2013.

[8] P. Senanayake *et al.*, "Thin 3D multiplication regions in plasmonically enhanced nanopillar avalanche detectors," *Nano Lett.*, vol. 12, no. 12, pp. 6448–6452, 2012.

[9] A. C. Farrell *et al.*, "InGaAs–GaAs nanowire avalanche photodiodes towards single-photon detection in free-running mode," *Nano Lett.*, vol. 19, no. 1, pp. 582–590, 2019.

[10] S. C. L. Mun, C. H. Tan, Y. L. Goh, A. R. J. Marshall, and J. P. R. David, "Modelling of avalanche multiplication and excess noise factor in In0.52Al0.48As avalanche photodiodes using a simple Monte Carlo model," *J Appl. Phys.*, vol. 104, no. 1, pp. 013114-1–013114-6, 2008.

[11] R. J. McIntyre, "Multiplication noise in uniform avalanche diodes," *IEEE Trans. Electron. Dev.*, vol. ED-13, no. 1, pp. 164–166, Jan. 1966.

[12] D. S. Ong, K. F. Li, G. J. Rees, J. P. R. David, and P. N. Robson, "A simple model to determine multiplication and noise in avalanche photodiodes," *J. Appl. Phys.*, vol. 83, no. 6, pp. 3426–3428, 1998.

[13] A. C. Farrell *et al.*, "Plasmonic field confinement for separate absorption-multiplication in InGaAs nanopillar avalanche photodiodes," *Sci. Rep.*, vol. 5, no. 1, pp. 17580-1–17580-6, 2015.

[14] X. Zhou, J. S. Ng, and C. H. Tan, "A simple Monte Carlo model for prediction of avalanche multiplication process in silicon," *J. Instrum.*, vol. 7, no. 8, pp. P08006-1–P08006-10, 2012.

[15] J. D. Petticrew, S. J. Dimler, X. Zhou, A. Morrison, C. H. Tan, and J. S. Ng, "Avalanche breakdown timing statistics for silicon single photon avalanche diodes," *IEEE J. Sel. Topics Quantum*, vol. 24, no. 2, pp. 1–6, Mar./Apr. 2018.

[16] S. A. Plimmer, J. P. R. David, D. S. Ong, and K. F. Li, "A simple model for avalanche multiplication including deadspace effects," *IEEE Trans Electron Device*, vol. 46, no. 4, pp. 769–775, Apr. 1999.

[17] C. H. Tan, R. Ghin, J. P. R. David, G. J. Rees, and M. Hopkinson, "The effect of dead space on gain and excess noise in In0.48Ga0.52P pin diodes," *Semi. Sci. Techn.*, vol. 18, no. 8, pp. 803–806, 2003.

[18] L. V. Keldysh, "Kinetic theory of impact ionization in semiconductors," *J. Exp. Theoretical Phys.*, vol. 10, no. 3, pp. 509–518, Mar. 1960.

[19] C. Groves, R. Ghin, J. P. R. David, and G. J. Rees, "Temperature dependence of impact ionization in GaAs," *IEEE Trans. Electron. Devices*, vol. 50, no. 10, pp. 2027–2031, Oct. 2003.

[20] 2018. [Online]. Available: https://www.lumerical.com/products/

[21] P. A. Alekseev *et al.*, "Nitride surface passivation of GaAs nanowires: Impact on surface state density," *Nano Lett.*, vol. 15, no. 1, pp. 63–68, Jan. 2015.

[22] J. S. Blakemore, "Semiconducting and other major properties of gallium arsenide," *J. Appl. Phys.*, vol. 53, no. 10, pp. 123–181, Oct. 1982.

[23] V. L. Dalal, A. B. Dreeben, and A. Triano, "Temperature dependence of hole velocity in p-GaAs," *J. Appl. Phys.*, vol. 42, no. 7, pp. 2864–2867, Jun. 1971.

[24] S. Yanikgonul, V. Leong, J. R. Ong, C. E. Png, and L. Krivitsky, "2D Monte Carlo Simulation of Silicon waveguide-based single photon avalanche diodes for visible wavelength," *Opt. Express*, vol. 26, no. 12, pp. 15232–15246, Jun. 2018.

[25] 2007. [Online]. Available: http://www.micro-photon-devices.com/Docs/Datasheet/PDM.pdf

[26] X. Collins, A. P. Craig, T. Roblin, and A. R. J. Marshall, "Impact ionisation in Al0.9Ga0.1As0.08Sb0.92 for Sb-based avalanche photodiodes," *Appl. Phys. Lett.*, vol. 112, no. 2, pp. 021103-1–021103-4, Jan. 2018.

[27] G. A. M. Hurkx, D. B. M. Klaassen, and M. P. G. Knuvers, "A new recombination model for device simulation including tunneling," *IEEE Trans. Electron Devices*, vol. 39, no. 2, pp. 331–338, Feb. 1992.

[28] S. Xie, H. Kim, W. J. Lee, A. C. Farrell, J. P. R. David, and D. L. Huffaker, "InAs/InAsP core/shell nanowire photodiode on a Si substrate," *Nano Adv.*, vol. 1, no. 3, pp. 110–114, 2016.

[29] D. Ren *et al.*, "Uncooled photodetector at short-wavelength infrared using InAs nanowire photoabsorbers on InP with p-n heterojunctions," *Nano Lett.*, vol. 18, no. 12, pp. 7901–7908, Dec. 2018.

[30] C. H. Tan, J. S. Ng, G. J. Rees, and J. P. R. David, "Statistics of avalanche current buildup time in single-photon avalanche diodes," *IEEE J. Sel. Topics Quantum Electron.*, vol. 13, no. 4, pp. 906–910, Jul./Aug. 2007.

[31] F. Najafi *et al.*, "On-chip detection of non-classical light by scalable integration of single-photon detectors," *Nature Commun.*, vol. 6, no. 1, pp. 5873-1–5873-8, Jan. 2015.

[32] M. S. Tyagi, "Zener and avalanche breakdown in silicon alloyed p-n junctions —I: Analysis of reverse characteristics," *Solid-State Electron.*, vol. 11, no. 1, pp. 99–115, Jan. 1968.